Distinct Mutants of Retrograde Intraflagellar Transport (IFT) Share Similar Morphological and Molecular Defects

Gianni Piperno,* Edward Siuda,* Scott Henderson,* Margarethe Segil,* Heikki Vaananen,‡ and Massimo Sassaroli‡

*Department of Cell Biology and Anatomy and ‡Department of Physiology and Biophysics, Mount Sinai School of Medicine, New York, 10029

Abstract. A microtubule-based transport of protein complexes, which is bidirectional and occurs between the space surrounding the basal bodies and the distal part of *Chlamydomonas* flagella, is referred to as intraflagellar transport (IFT). The IFT involves molecular motors and particles that consist of 17S protein complexes. To identify the function of different components of the IFT machinery, we isolated and characterized four temperature-sensitive (ts) mutants of flagellar assembly that represent the loci *FLA*15, *FLA*16, and *FLA*17. These mutants were selected among other ts mutants of flagellar assembly because they displayed a characteristic bulge of the flagellar membrane as a nonconditional phenotype. Each of these mutants was significantly defective for the retrograde velocity of particles and the frequency of bidirectional transport but not for the anterograde velocity of particles, as revealed by a novel method of analysis of IFT that allows tracking of single particles in a sequence of video images. Furthermore, each mutant was defective for the same four subunits of a 17S complex that was identified earlier as the IFT complex A. The occurrence of the same set of phenotypes, as the result of a mutation in any one of three loci, suggests the hypothesis that complex A is a portion of the IFT particles specifically involved in retrograde intraflagellar movement.

Key words: *Chlamydomonas* • temperature-sensitive mutants • intraflagellar particles • video microscopy • retrograde transport

TRANSPORT of proteins from the site of synthesis to the site of function in eukaryotic cells often occurs along frameworks of microtubules with the participation of molecular motors and auxiliary molecules that link the motors to the cargo. These molecular machineries also operate in specific compartments of polarized cells, such as cilia, flagella, and axons, where they serve several functions: among others, they release a cargo at the distal part of the compartment and move back to the cell body to be recycled. Retrograde transport often requires molecular motors that differ from those working in anterograde transport.

To dissect the complexity of a microtubule-based system that transports proteins within a specific cellular compartment, we turned to the study of temperature-sensitive (ts)[1] mutants of *Chlamydomonas reinhardtii* that are defective in the assembly of flagella (Huang et al., 1977). *Chlamydomonas* flagella contain a machinery that transports protein complexes in both directions and operates between outer doublet microtubules and the flagellar membrane (Kozminski et al., 1995). This intraflagellar transport (IFT) of protein particles was discovered by video-enhanced differential interference contrast microscopy (Kozminski et al., 1993) and currently is being analyzed at the molecular level (Piperno and Mead, 1997; Cole et al., 1998; Pazour et al., 1998).

The IFT requires KHP1^{FLA10} (Walther et al., 1994), the heavy chain of an heterotrimeric kinesin II (Scholey, 1996), for anterograde transport (Kozminski et al., 1995; Cole et al., 1998) and LC8^{FLA14}, a light chain of axonemal and cytoplasmic dyneins (King et al., 1996), for retrograde transport of a cargo (Pazour et al., 1998). The cargo consists of large protein particles that are not membrane-bound (Kozminski et al., 1995) and are composed of at least 15 polypeptides comprising two 16S complexes, referred to as IFT complexes A and B (Cole et al., 1998).

Following our studies on the structure of inner dynein

Address correspondence to Gianni Piperno, Department of Cell Biology and Anatomy, Mount Sinai School of Medicine, 1 Gustave Levy Place, Box 1007, New York, NY 10029. Tel.: (212) 241-0773. Fax: (212) 860-1174. E-mail: Piperno@msvax.mssm.edu

1. *Abbreviations used in this paper:* IFT, intraflagellar transport; MNNG, *N*-methyl-*N*′-nitro-*N* nitrosoguanidine; ts, temperature-sensitive.

arms, we analyzed the transport of p28, an inner dynein arm light chain, within the flagella of *ida*4 (Piperno et al., 1996), a null mutant of p28 (LeDizet and Piperno, 1995*a*). We found that p28 required KHP1^{FLA10} to reach the distal part of flagella where it bound to outer doublet microtubules in a concentration gradient from distal to proximal part of the axoneme. This evidence suggested that the transport of precursors of inner dynein arms to their binding site within the axoneme involved a molecular motor and not passive diffusion (Piperno et al., 1996).

We also found that a cytoplasmic 17S complex of polypeptides binds p28 in substoichiometric amounts and requires KHP1^{FLA10} to be present in flagella (Piperno and Mead, 1997). The 17S complex represents 2–4% of the mass of flagellar proteins and is composed of at least 13 different subunits, nine of which turned over 37 times faster than axonemal dyneins (Piperno and Mead, 1997). This evidence suggested the following hypotheses: the 17S complex functions as a carrier of precursors of inner dynein arms and consists of two modules that differ in turnover (Piperno and Mead, 1997). Furthermore, the 17S complex is probably identical to the ensemble of the IFT complexes A and B recently described (Cole et al., 1998).

To identify the function of different parts of this machinery of transport, we intended to isolate ts mutants of flagellar assembly with a defect in a specific aspect of the IFT, such as the anterograde motion, the retrograde motion, or the frequency of transport. To this purpose we analyzed ts mutants of flagellar assembly with phenotypes similar to that of *fla*10 because the IFT is inhibited at the restrictive temperature in flagella of *fla*10 (Kozminski et al., 1995), and KHP1^{FLA10} and the 17S complex are parts of the same transport system (Kozminski et al., 1995; Piperno and Mead, 1997; Cole et al., 1998). In an initial phase of this study, we observed ts mutants isolated by others (Huang et al., 1977; Adams et al., 1982). However, some of them lost the original ts phenotype while others could have accumulated additional mutations. Therefore, instead of characterizing them again we isolated a new set of ts mutants of flagellar assembly by a procedure that is similar to that previously described (Huang et al., 1977; Adams et al., 1982). Furthermore, to detect subtle changes in a specific property of the IFT, we developed a method of quantitative analysis of the IFT that allows unambiguous identification of single particles and, therefore, accurate measurement of anterograde and retrograde velocity of the particles.

Here we describe four of the new ts mutants of flagellar assembly, which we selected from among the others because they have an additional phenotype, namely a distinct bulge of the flagellar membrane. These four mutants represent three loci referred to as *FLA*15, *FLA*16, and *FLA*17. They have flagella as long as those of a wild-type strain at permissive temperature and accumulated amorphous material in the flagellar bulge at both permissive and restrictive temperatures. The presence of the flagellar bulge in each mutant was correlated with a decrease of both velocity of retrograde IFT and frequency of bidirectional transport. In addition, each mutant was defective for the same four subunits of a 17S complex, three of which were identified earlier as subunits of the IFT complex A. The identification of the gene products of *FLA*15, *FLA*16, and *FLA*17 should reveal whether IFT complex A is required for retrograde transport of protein particles within flagella.

Materials and Methods

Cell Culture

Wild-type cells (137$^+$) used for mutagenesis were grown in liquid medium (Sager and Granick, 1953) as modified in Huang et al. (1977) for 3 d under intense light at 25°C. Wild-type cells (137$^+$) or mutants used for biochemical or phenotypic analyses were grown on solid medium for 3 d under intense light at 25°C and 1 d in the dark at 21°C. Cells used for phenotypic analysis were cultured in liquid medium for at least 12 h under light at 21°C.

Proteins were extracted from wild-type cells (137$^+$) or mutants that were grown at a steady state on modified solid medium supplemented with [^{35}S]sulphuric acid (Luck et al., 1977).

The wild-type strains 137 and *fla*10-1 are from the collection of Dr. David Luck (Rockefeller University, New York).

Screening of Temperature-sensitive Mutants for Flagellar Assembly

Vegetative wild-type cells (137$^+$, 10^6 cells/ml) in 50 ml of 0.02 M citrate buffer, pH 5, were exposed to 1, 5, or 10 mg/ml of *N*-methyl-*N*′-nitro-*N* nitrosoguanidine (MNNG) for 30 min at 25°C in the dark. After two washes in medium, cells (10^6 cells/ml) were cultured for 24 h in light at 21°C. Survival was 71, 57, and 45% after the exposure to 1, 5, or 10 mg/ml of MNNG, respectively. Screening of temperature-sensitive mutants for flagellar assembly was achieved by three repeats of the following two-step cycle: we discarded cells regenerating their flagella and swimming at the restrictive temperature of 32°C, and we also discarded cells not swimming at the permissive temperature of 21°C. At the first step of the cycle, cells were deflagellated by pH shock, pelleted by centrifugation at 1,000 rpm (in a model GH-3.7 rotor; Beckman Instruments, Fullerton, CA), resuspended in 30 ml of medium, and exposed 3 h at 32°C in light before being separated in four aliquots, one of which was enriched in cells that were sedimenting. Sedimenting cells were cultured overnight at 21°C in light. After this incubation, the upper 70% of the culture was removed and kept for the next screening at 32°C. The volumes of the medium added to the cells before the second and third exposure at 32°C were 5 and 3 ml, respectively. We cultured the remaining cells in solid medium, picked single colonies, and cultured them in 200 μl of liquid medium. We selected clones that lost the majority of their flagella within 4 h of exposure at 32°C. We retained 11 and 5 clones of mutants from cells exposed to 1 or 5 mg/ml of MNNG, respectively. Some of the clones could derive from the same mutant that divided during the process of screening.

Mutants in four distinct clones had the same phenotype: a bulge of the flagellar membrane. They were crossed with wild-type cells (137$^-$) to verify that they represented a single mutation. They also were crossed to each other and to *fla*10 to determine whether they represented different loci. Complementation tests were performed by tetrad analysis (Harris, 1989). Three of the four mutants recombined and generated wild-type cells in reciprocal crosses. In contrast, two mutants did not recombine in 204 crosses. Each of the three mutants that recombined also recombined with *fla*10. Therefore, the four mutants were referred to as *fla*15, *fla*16, *fla*17-1, and *fla*17-2 to follow the nomenclature previously adopted for temperature-sensitive mutants of flagellar assembly (Adams et al., 1982; Harris, 1989). Whether any one of these mutants is an allele of a *fla* mutant other than *fla*10 remains to be determined.

Recombinant strains between *pf*15, a paralyzed flagella mutant (Adams et al., 1981), and *fla*10, *fla*15, *fla*16, and *fla*17-1 were isolated to carry out the analysis by video microscopy. They had straight, immotile flagella and were temperature-sensitive for flagellar assembly.

Optical and Video Microscopy

Phenotypic analysis of mutants was performed on cells fixed in 2% glutaraldehyde, 0.01 M sodium phosphate buffer, pH 6.9. Phase contrast microscopy was performed with a microscope (model Axioskop; Carl Zeiss, Inc., Thornwood, NY) connected to a CCD camera (SenSys, model KAF 1400; Photometrics, Tucson, AZ) through a 4× intermediate lens.

Differential interference contrast microscopic observation of intraflagellar transport of particles in living cells was carried out using a microscope (model Axiovert 35; Carl Zeiss, Inc.) with a 1.4 NA condenser, a

100×, 1.3 NA Plan Neofluar objective, and a 4× magnifier placed on the trinocular head in front of a video camera equipped with a Newvicon tube (model C2400-07; Hamamatsu Corporation, Bridgewater, NJ). Transillumination light was provided by a mercury arc and filtered through a Zeiss standard green filter. Video images were acquired at a rate of 30 frames/s and stored directly on optical disks (model TQ-3038F Optical Disc Recorder; Panasonic Communications and Systems Company, Secaucus, NJ). Calibration of pixel dimensions was carried out by use of a stage micrometer.

Cells in liquid medium were immobilized in ~0.25% low melting temperature agarose (SeaPlaque; FMC BioProducts, Rockland, ME) in a thin chamber created by a glass coverslip and a slide held together by Scotch double-side adhesive tape that also served as a spacer.

Quantitative Analysis of Intraflagellar Transport of Particles

Measurement of the velocities of bidirectional intraflagellar transport of particles was carried out by a new method that does not rely on image contrast enhancement and subtraction of successive images as previously described (Kozminski et al., 1995; Pazour et al., 1998). Each image in a video sequence was read from the optical disc recorder and digitized by a frame grabber. A light intensity profile, or linescan, along the flagellum was obtained using a built-in function of the Image-1 software package (Universal Imaging Corporation, West Chester, PA). To increase the signal-to-noise ratio, the values of five pixels across the width of the flagellum were averaged for each value in the linescan. The position of each individual particle was identified by a sinusoidal deflection around the local mean signal intensity in the linescan. The amplitude of this deflection, or contrast, and its length are functions of the birefringence of the particle, its size as well as its distance from the focal plane. Under our conditions, the peak-to-peak amplitude of these features was ~1–2% of the total signal. Direct visualization of particles undergoing bidirectional motion was obtained by means of a composite plot obtained by simply adding an offset to each linescan to displace it from the preceding one and displaying the whole sequence as a stack. The intensity dimension in this composite plot also contained time information since the stacked linescans were derived from images obtained at 33-ms intervals. In these plots, moving particles appeared as diagonal ridges or streaks, whose slope was proportional to their velocity. Although the raw linescans were sufficient to identify and track many of the particles moving in the anterograde direction, which usually display stronger contrast, they were not suitable for a complete analysis of the data and an accurate measurement of bidirectional particle velocities because of several factors, such as the presence of uneven background, light intensity fluctuations, and digitization noise. To overcome these limitations, the data were submitted to singular value decomposition, a mathematical procedure that yields a reduced representation of the original data in terms of a set of n_s nonzero eigenvalues, also called singular values, and two sets of orthogonal eigenvectors (Golub and Reinsch, 1970; Malinowski, 1991; Press et al., 1992). The first set of eigenvectors constitutes a matrix **U** with dimensions $n_s \times p$, where p is the number of pixels in each linescan and is formed by n_s component "spectra" or waveforms, which carry information related to the shape of the experimental linescans. The second set of eigenvectors forms a matrix **V** with dimensions $n_s \times l$, where l is the number of linescans and carries information about the fractional contribution of each of the n_s components to each of the linescans. Finally, each of the n_s singular values in the diagonal matrix **S** measures the weight or contribution of the respective component to the ensemble of linescans. Multiplication of the three matrices, $\mathbf{USV^T}$, where $\mathbf{V^T}$ represents the transpose of **V**, using the complete set of eigenvalues and eigenvectors yielded a perfect reproduction of the original ensemble of linescans, including background and noise. However, inspection of the **U** eigenvectors revealed that components beyond the first 10–20 contained uncorrelated signal arising from noise in the data, whereas the first, and sometimes up to the third, eigenvector contained the signal contribution of the structured background. Matrix multiplication using the subset of intermediate components yielded a reconstructed ensemble of linescans in which the contributions of both background and noise were suppressed. As a result, this procedure not only allowed the unambiguous identification of moving particles but also eliminated the distortions in the time component of the time/intensity dimension caused by variations in the signal due to fluctuations in light intensity and other artifacts present in the unprocessed data. Examples of composite plots of linescans from the flagellum of *pf*15, a mutant with straight and immotile flagella that was used as a reference strain, and of *fla*15*pf*15, one of the recombinant strains characterized in this study, are shown in Fig. 4. The velocity of each particle was calculated from the slope of a line drawn manually along each of the diagonal ridges.

A lower limit for the value of the frequency of intraflagellar transport, expressed in particles/second, was estimated from the ratio of the total number of particles detected to the total observation time, equal to the number of linescans divided by thirty, the video frame rate. The frequency of retrograde transport probably was underestimated as a result of the lower contrast generated by particles moving in that direction, whose features in the composite plots were therefore at the limit of detection.

Electron Microscopy

Cells were fixed in 3% glutaraldehyde in 10 mM Hepes buffer, pH 7.2, for 2 h at 4°C. The fixed cells were then washed three times for 10 min each in 10 mM Hepes buffer, pH 7.2, and postfixed in 1% OsO_4 plus 0.8% $K_3Fe(CN)_6$ in 4 mM phosphate buffer, pH 7.2, for 30 min at 4°C (McDonald, 1984). The cells were then washed with water for 10 min, stained with 0.15% tannic acid for 1 min, again washed with water for 10 min, and stained en bloc in 2% uranyl acetate for 1 h at room temperature in the dark. After staining, the cells were washed with water for 10 min and then dehydrated through a graded ethanol series (70, 80, 90, 100, and 100%, 30 min in each stage). The cells were taken through a transition of propylene oxide for 15 min and 1:1 propylene oxide:epon/araldite resin for 1 h at room temperature on a rotator. They were then infiltrated with epon/araldite resin overnight at room temperature on a rotator and, finally, embedded in a fresh batch of epon/araldite resin. The resin was polymerized at 68°C for 2 d.

Silver sections were cut on an Ultracut E ultramicrotome (Reichert-Jung, Vienna, Austria), collected on 200 mesh grids, and stained with uranyl acetate for 20 min and lead citrate for 2 min. Examination and photography of sections was carried out using a transmission electron microscope (model H-7000; Hitachi, Tokyo, Japan).

Isolation of the 17S Complex

Flagella were separated from the cell bodies by a pH shock method (Huang et al., 1979). After ultrasonic disruption of flagella, soluble proteins were separated from the insoluble residue by centrifugation at 14,000 rpm in a table top minicentrifuge (model 5402; Eppendorf, Madison, WI). Protein fractions containing the 17S complexes were isolated by sedimentation in a 5–20% sucrose gradient (Piperno and Mead, 1997). Sedimentation standards were 21S and 11S *Chlamydomonas* dyneins (Piperno et al., 1990) that were sedimented either with the flagellar extracts or in a parallel gradient.

Chromatography on a DEAE-Sepharose column (fast flow, Pharmacia Biotech, Piscataway, NJ) was carried out on a 0.3-ml column. Elution of proteins was performed by a 4-ml 0.03–0.4 M NaCl gradient in 0.01 M Hepes, pH 6.8. The concentration of the salt gradient was measured by refractometry.

Gel Electrophoresis of Polypeptides

One- and two-dimensional electrophoresis of ^{35}S-labeled polypeptides were carried out as described (Piperno, 1995) with the following two modifications. SDS gels were made of a 4–11% polyacrylamide gradient. Isoelectric focusing was carried out either at 1.4 mA for 14 h or 1.6 mA for 16 h. Quantitative analysis of the isoelectric point was carried out under the second set of conditions, which allowed the subunits of the 17S complex to reach their isoelectric point. Determination of pH of the gel containing polypeptides at their isoelectric point was carried out directly in suspensions of 1 × 1 × 0.1 cm gel slices in 2 ml of water.

Evaluation of apparent molecular weight of polypeptides was performed by the use of molecular weight standards (Pharmacia Biotech lot 7070615011 and GIBCO-BRL lot KB9418). The values reported here for 13 subunits of the 17S complex were: (*1*) 189,000; (*2*) 148,000; (*3*) 127,000; (*4*) 86,000; (*5*) 81,000; (*6*) 71,000; (*7*) 69,000; (*8*) 65,000; (*9*) 56,000; (*10*) 47,000; (*11*) 26,000; (*12*) 21,000; and (*13*) 19,000. These values are probably more accurate than those reported before (Piperno and Mead, 1997). The previous set of data was obtained by prestained molecular weight standards (SDS-7B lot 125H9408; Sigma Chemical Co., St. Louis, MO) that yielded nonreproducible results.

Western Blots

Western blot analyses of axonemal proteins and subunits of the 17S were

performed as described (LeDizet and Piperno, 1995*b*). To detect the presence of inner dynein arms, outer dynein arms, and central pair complexes in flagella from *fla*15, *fla*16, and *fla*17-1, we used antibodies specific for p28 (LeDizet and Piperno, 1995*b*), γ-chain of outer dynein arms (Piperno et al., 1996), and *PF*16 gene product (Smith and Lefebvre, 1996), respectively. Equal amounts of axonemal proteins from each mutant and a wild-type strain bound each antibody in similar amounts. To identify subunit 2 of the 17S complex (Piperno and Mead, 1997) with p144–p139 subunits of complex A (Cole et al., 1998), we used monoclonal antibody 139.1 (Cole et al., 1998).

Results

Temperature-sensitive Mutants of Flagellar Assembly with a Nonconditional Phenotype: A Bulge of the Flagellar Membrane

To identify ts mutants of flagellar assembly that are defective in the IFT, we generated mutants similar to *fla*10, a ts mutant of a motor involved in IFT (Walther et al., 1994; Kozminski et al., 1995; Cole et al., 1998). After mutagenesis and screening, we isolated 16 strains that lost or did not regenerate their flagella after 4 h of exposure at the restrictive temperature of 32°C. Four strains also had a nonconditional phenotype: a distinct bulge of the flagellar membrane. We selected these four strains for further analysis because such a deformation of the flagellar membrane could derive from disruptions in the transport of protein particles that occurs between outer doublet microtubules and the flagellar membrane (Kozminski et al., 1995).

We performed a complementation test on the four strains and found that three of them consisted of mutants representing different loci. Therefore, we will refer to the four mutants as *fla*15, *fla*16, *fla*17-1, and *fla*17-2, following the designation used for mutants of flagellar assembly (Adams et al., 1982). The strain *fla*17-2 was not used as extensively as *fla*17-1 in the following studies because it may be a clone of the same mutation in *FLA*17, as explained in Materials and Methods.

Anomalous assembly of flagella in *fla*15, *fla*16, and *fla*17-1 was evident at both permissive and restrictive temperatures. At the permissive temperature, we detected a defect in flagellar assembly by measuring the rate of regeneration of flagella. Increasing delay in the regeneration of flagella was observed in the following order: *fla*15 > *fla*16 > *fla*17-1 > wild-type (Fig. 1). However, the final length of the regenerated flagella in all mutants was similar to that of the wild-type strain (Fig. 1). Therefore, mutations in *FLA*15, *FLA*16, and *FLA*17 affected the rate of assembly of flagella, not the control of flagellar length.

A 4-h exposure of each mutant to the restrictive temperature led to extensive loss of flagella similar to that observed in *fla*10 (Table I). The flagella remaining in mutants following a 4-h exposure to the restrictive temperature were ~50% shorter than in a wild-type strain (Table I). Prolonged exposures (6–8 h) to the restrictive temperature caused complete retraction of flagella in the mutant cells.

In contrast to *fla*10, which has wild-type–like flagella at the permissive temperature, *fla*15, *fla*16, *fla*17-1, and *fla*17-2 have a bulge positioned randomly along the length of one flagellum at both permissive and restrictive temperatures but not in isolated flagella. Occasionally, the bulge was on both flagella or was absent. Its short diameter was ~0.4 μm, near the limit of the optical microscope resolution. The bulge was immotile at least over the time course of microscopic observation, 5–10 min. Examples of bulges on the flagellar membrane of *fla*15 are shown in Fig. 2, as detected by differential interference and phase contrast microscopy after fixation in glutaraldehyde. The other mutants were indistinguishable from *fla*15 by this criterion.

Electron microscopy of *fla*15, *fla*16, and *fla*17-1 revealed that the bulge of the flagellar membrane contained amor-

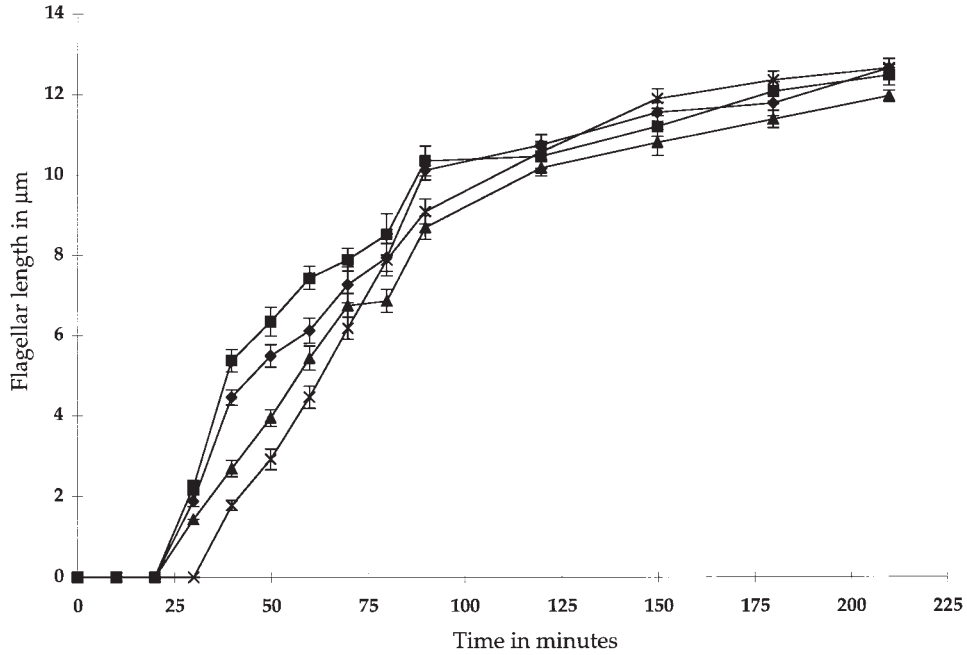

Figure 1. Flagellar assembly of temperature-sensitive mutants *fla*15, *fla*16, and *fla*17-1 was defective at permissive temperature. A wild-type strain and *fla*15, *fla*16, and *fla*17-1 were cultured, deflagellated by pH shock, and analyzed by phase contrast microscopy during the regeneration of flagella at permissive temperature. The length of flagella was measured after fixation. Vertical bars represent the standard error of the mean of 25 determinations. *Squares*, wild-type; *diamonds*, *fla*17-1; *triangles*, *fla*16; *X*, *fla*15.

Table I. Loss of Flagella after a 4-h Exposure at Restrictive Temperature

Strain	Flagellated cells		Length of flagella	
	21°C	32°C	21°C	32°C
			μm	
137^+	87.3% (*n*: 102)	76.9% (*n*: 147)	11.5 (*s*: 0.2; *n*: 25)	11.1 (*s*: 0.2; *n*: 25)
*fla*10	91.0% (*n*: 100)	16.3% (*n*: 147)	11.7 (*s*: 0.1; *n*: 25)	6.6 (*s*: 0.3; *n*: 25)
*fla*15	83.3% (*n*: 132)	11.8% (*n*: 153)	11.0 (*s*: 0.3; *n*: 25)	6.0 (*s*: 0.3; *n*: 25)
*fla*16	68.5% (*n*: 124)	19.0% (*n*: 199)	10.1 (*s*: 0.4; *n*: 25)	5.4 (*s*: 0.3; *n*: 25)
*fla*17-1	48.6% (*n*: 138)	9.4% (*n*: 107)	11.1 (*s*: 0.2; *n*: 25)	5.8 (*s*: 0.3; *n*: 25)

n, number of determinations; *s*, standard error of the mean.

phous material that was concentrated between the flagellar membrane and the outer doublet microtubules (Fig. 3) and was indistinguishable from cytoplasm. Axonemal substructures, such as the central pair complex, radial spokes, and dynein arms, had normal morphology in both cross and longitudinal sections. Therefore, mutations in *FLA*15, *FLA*16, and *FLA*17 affected the flagellar shape but not the axonemal structure.

The absence of a marked axonemal defect was confirmed by two independent lines of evidence. Two-dimensional maps of axonemal polypeptides from *fla*15 and a wild-type strain were indistinguishable. In addition, the presence of outer dynein arms, inner dynein arms, and central pair complexes in axonemes of *fla*15, *fla*16, and *fla*17-1 was confirmed by immunoblots of axonemal proteins using antibodies specific for a protein subunit of each of these axonemal substructure, as described in Materials and Methods.

Retrograde but Not Anterograde Transport of Particles Is Defective in Flagella of fla15, fla16, and fla17-1

To determine whether IFT is inhibited in *fla*15, *fla*16, and *fla*17-1, as it is in *fla*10 at the restrictive temperature (Kozminski et al., 1995), we observed flagella in vivo by video-enhanced differential interference contrast microscopy. For this purpose, we isolated recombinants between the mutants and *pf*15, a paralyzed flagella mutant, to perform the microscopic analysis on immotile and straight flagella. In each recombinant, *fla*10*pf*15, *fla*15*pf*15, *fla*16*pf*15, and *fla*17-1*pf*15 transport was seen to occur along the whole length of the flagella, including the section where the membrane swelling was located.

Quantitative analysis of the velocity and the frequency of IFT of protein particles in both anterograde and retrograde directions was carried out by a new method described in Materials and Methods. The analysis required both the scanning of light intensity along a flagellum in each video frame and the composition of linescans. In these composite plots, moving particles appear as diagonal ridges or streaks, whose slope is proportional to their velocity. Examples of these streaks originating from particles undergoing anterograde and retrograde transport were colored in red and green, respectively, in the composite plots generated with *pf*15 and *fla*15*pf*15 (Fig. 4). Particles undergoing anterograde transport generated a stronger light contrast than particles undergoing retrograde transport. Therefore, these particles differed in optical properties from those moving in the opposite direction.

At the permissive temperature, the velocity of anterograde movement of particles in *pf*15 was similar to that in *fla*10*pf*15, *fla*15*pf*15, *fla*16*pf*15, and *fla*17-1*pf*15 (Table II). In contrast, the velocity of retrograde transport in *fla*15 *pf*15, *fla*16*pf*15, and *fla*17-1*pf*15 was significantly lower than that in *pf*15 and *fla*10*pf*15 (Table II). Results of these comparisons between each recombinant and *pf*15 are significant at a confidence level of $P < 0.001$, as determined by standard Student's *t* test.

At the restrictive temperature, the velocity of retrograde transport of particles did not change significantly in *fla*16*pf*15 and *fla*17-1*pf*15, whereas retrograde transport was undetectable in the majority of *fla*10*pf*15 flagella and in all *fla*15*pf*15 flagella.

The representative plots of singular value decomposition processed linescans measured from *pf*15 and *fla*15 *pf*15 at the permissive temperature (Fig. 4) show that the

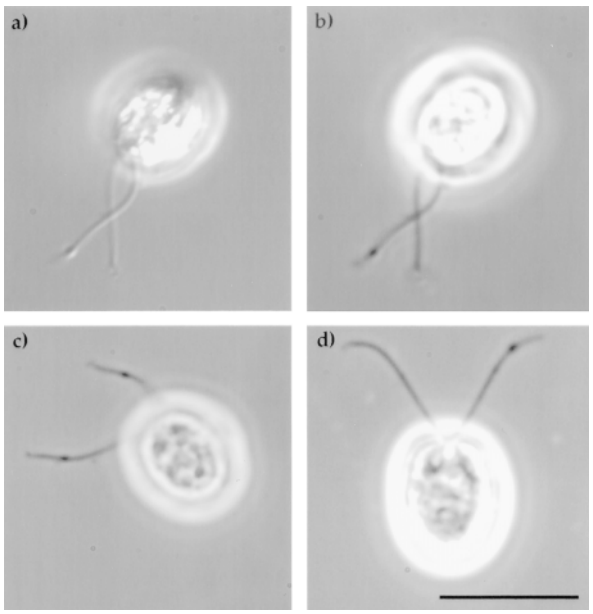

Figure 2. *fla*15 caused a bulge of the flagellar membrane. Micrographs of *fla*15 cultured and fixed at permissive temperature. (*a*) Differential interference contrast micrographs. (*b–d*) Phase contrast micrographs. Bar, 10 μm.

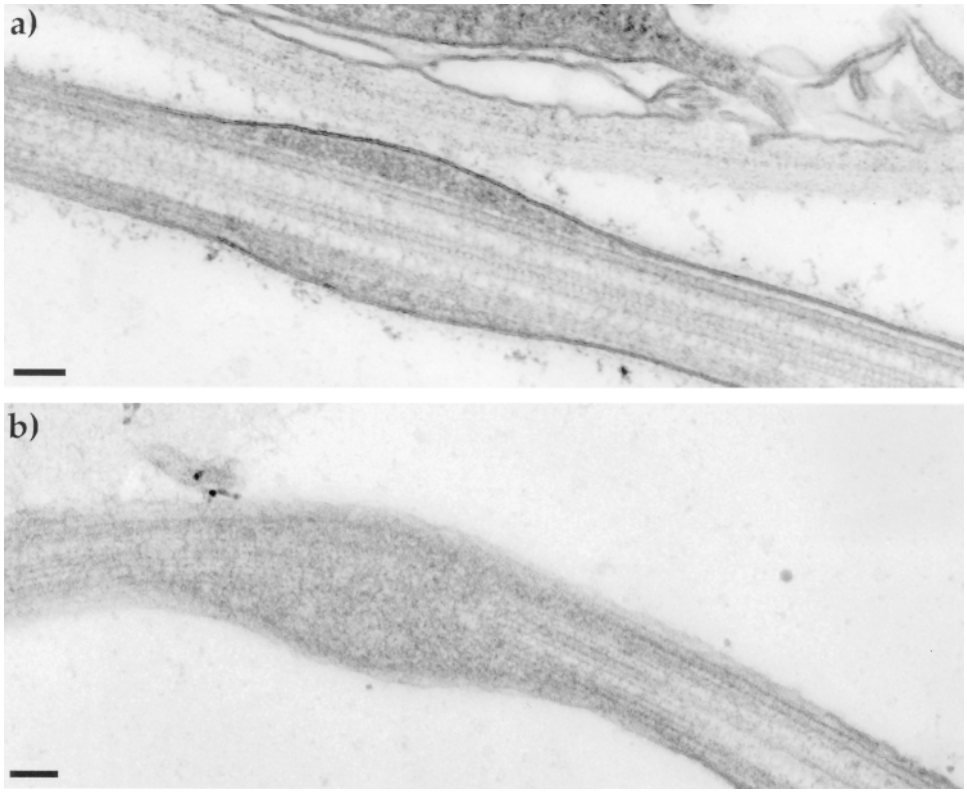

Figure 3. The deformation of the flagellar shape caused by *fla*15 was correlated with the accumulation of cytoplasmic matrix. (*a* and *b*) Electron micrographs. (*a*) Longitudinal section cut through the central pair microtubules. The cytoplasm accumulated between the outer doublet microtubules and the flagellar membrane in a section of the axoneme. (*b*) Longitudinal section cut through the cytoplasm accumulated in the bulge of the flagellar membrane. Bar, 0.1 μm.

frequency of bidirectional transport is decreased in *fla*15 *pf*15. The frequencies of bidirectional transport in *fla*15 *pf*15, *fla*16*pf*15, and *fla*17-1*pf*15 were 24, 66, and 51% of that of *pf*15, respectively. In contrast, the frequency of bidirectional IFT of *fla*10*pf*15 was similar to that of *pf*15 under the same condition.

In summary, *fla*15, *fla*16, and *fla*17-1 differ from *fla*10 for the presence of a bulge on their flagella, a lower veloc-

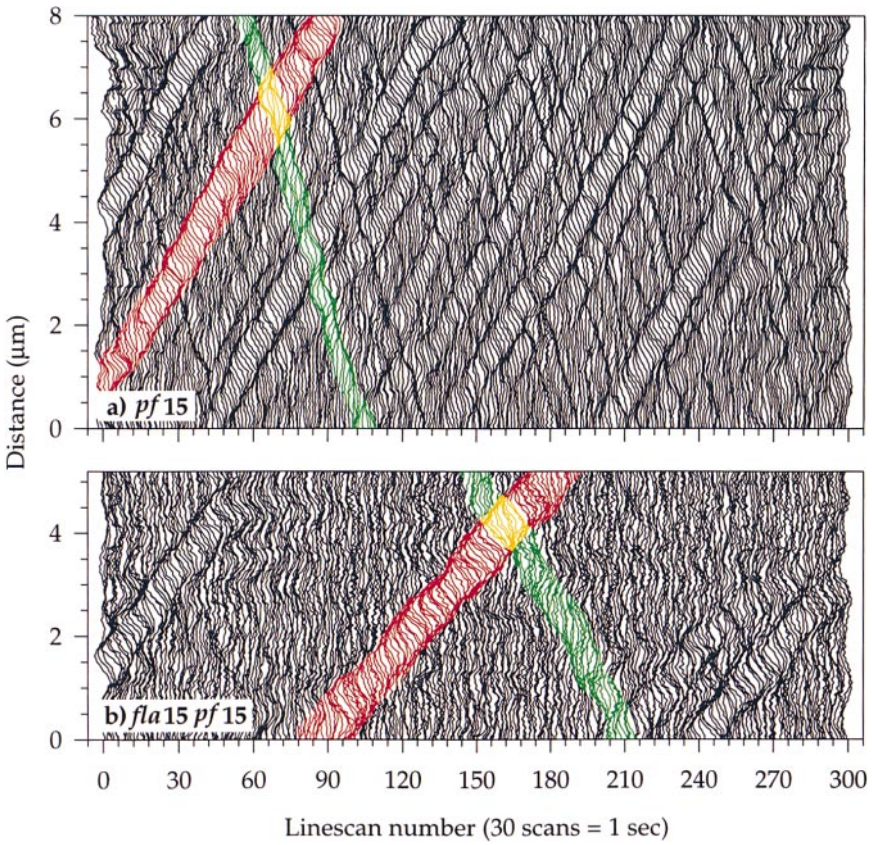

Figure 4. Representative illustration of intraflagellar transport of particles occurring at permissive temperature. Composite plots of longitudinal linescans of light intensity along flagella of (*a*) *pf*15 and (*b*) *fla*15*pf*15. One linescan from the proximal to the distal part of the flagellum was measured for each successive image in a video sequence obtained at a rate of 30 frames/s. The ensemble of linescans was then subjected to singular value decomposition and reconstructed as described in the text. The processed linescans were stacked and displayed so that the origin of the *x* axis corresponds to both the first linescan of a sequence and the proximal part of the flagellum. The distance on the *y* axis was measured relative to the proximal part of the flagellum. Particles undergoing anterograde or retrograde transport are identifiable as ridges with rightward and leftward slopes, respectively. (*a* and *b*) Examples of red and green ridges represent particles undergoing anterograde and retrograde transport, respectively.

Table II. Velocity of Intraflagellar Particles

Strain	Anterograde	Retrograde
	μm/s	
*pf*15	2.2 (SD: 0.3; *n*: 43)	3.9 (SD: 0.6; *n*: 32)
*pf*15*fla*10	1.8 (SD: 0.2; *n*: 64)	4.2 (SD: 0.6; *n*: 81)
*pf*15*fla*15	2.1 (SD: 0.3; *n*: 47)	2.9 (SD: 0.5; *n*: 17)
*pf*15*fla*16	2.1 (SD: 0.2; *n*: 104)	2.7 (SD: 0.6; *n*: 40)
*pf*15*fla*17-1	1.9 (SD: 0.3; *n*: 121)	2.3 (SD: 0.4; *n*: 36)

n, number of particles analyzed.

ity of retrograde IFT and a lower frequency of bidirectional transport. These phenotypes are nonconditional, in contrast to the lack of flagellar assembly or flagellar regeneration that is expressed at the restrictive temperature in every mutant including *fla*10.

fla15, fla16, and fla17-1 Are Deficient for the Same Subunits of the IFT Complex A

The *FLA*10 product is KHP1^{FLA10} (Walther et al., 1994), a subunit of a kinesin II (Scholey, 1996), and KHP1^{FLA10} and the 17S complex are parts of the same transport system within flagella (Kozminski et al., 1995; Piperno and Mead, 1997; Cole et al., 1998). To determine whether the 17S complex was defective in *fla*15, *fla*16, and *fla*17-1, we extracted it from flagella of each mutant grown at the permissive temperature. Under this condition, the concentration of the 17S complex in flagella of the mutants was similar to that of a wild-type strain. In contrast, the concentration of the 17S complex decreased several folds in flagella of mutants exposed to the restrictive temperature.

The sedimentation profiles of ^{35}S-labeled flagellar proteins from mutant strains were indistinguishable from that of a wild-type strain. However, the electrophoretograms of protein fractions from the sucrose gradients revealed that the 17S complexes from each mutant were deficient to a different extent for the same two polypeptides with apparent molecular weights of 148,000 and 127,000. The electrophoretic bands of defective polypeptides from *fla*15 are indicated by asterisks located between lanes *9* and *10* of the electrophoretograms (Fig. 5 *b*). The other subunits of 17S complexes from *fla*15 and a wild-type strain are indicated by lines (Fig. 5, *b* and *a*, respectively).

The polypeptides deficient from flagella of *fla*15, *fla*16, and *fla*17-1 had apparent molecular weights similar to those of two subunits of complex A (Cole et al., 1998) (Table III). Furthermore, in the absence of these polypeptides the sedimentation properties of the remaining subunits of the 17S complexes were not altered. Therefore, polypeptides that are defective from each mutant may form a distinct 17S complex in a wild-type strain, and this complex may be the IFT complex A (Cole et al., 1998).

To test these hypotheses and determine whether other deficiencies occur in each mutant, we separated the polypeptides of 17S sedimenting fractions from wild-type and mutant strains by high-resolution one- and two dimensional gel electrophoresis. In these experiments, we identified the 13 subunits of the two 17S complexes by their apparent molecular weights. These subunits are indicated by lines and progressive numbers in Fig. 6.

Flagella of *fla*15, *fla*16, and *fla*17-1 contained reduced amounts of subunits 2 and 3 relative to flagella of a wild-type strain (Fig. 6). In addition, flagella of *fla*15 lacked a polypeptide of apparent molecular weight 43,000, indicated by a line between *a* and *b* in Fig. 6. This polypeptide was not previously identified as a subunit of the 17S complex (Piperno and Mead, 1997) or complexes A and B (Cole et al., 1998). In contrast, flagella of *fla*16 and *fla*17-1 had reduced amounts of the 43,000 polypeptide and contained an additional polypeptide, apparent molecular weight 135,000, indicated by a dot between the second and third lanes in Fig. 6 *b*. This last polypeptide is absent in flagella of *fla*15 and of the wild-type (Fig. 6 *a*).

Comparison of two-dimensional electrophoretograms of

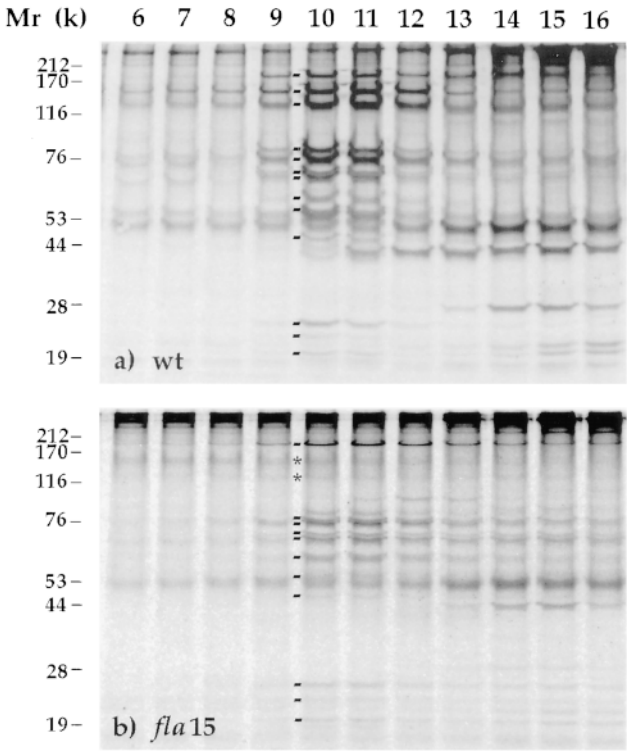

Figure 5. *fla*15 was defective for two polypeptides of the 17S sedimenting fractions from the cytoplasmic matrix of flagella. Autoradiograms of ^{35}S-labeled polypeptides contained in sucrose gradient fractions 6–16 after separation by gel electrophoresis. Molecular weight standards are indicated on the left. (*a*) Proteins from a wild-type strain. Lines between lanes *9* and *10* indicate the presence of components 1–13 of the two 17S complexes. (*b*) Proteins from *fla*15. Asterisks between lanes *9* and *10* indicate the position of the two polypeptides that are deficient in *fla*15. Lines indicate the rest of the subunits of 17S complexes.

Table III. Polypeptide Composition of IFT Complex A from a Wild-Type Strain

Cole et al., 1998		This study	
Apparent molecular weight	pI	Apparent molecular weight	pI
144,000	5.7–5.8	148,000	6.5
140,000	6.0	148,000	6.0
139,000	5.9	127,000	6.3
122,000	5.8–6.0	43,000	4.5

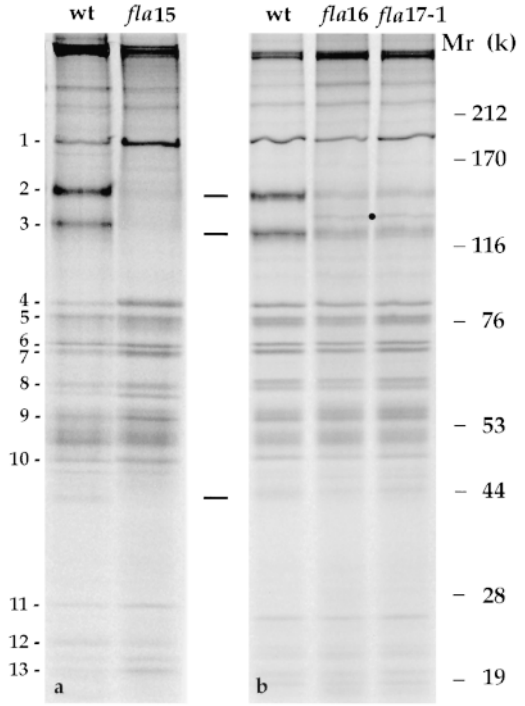

Figure 6. *fla*15, *fla*16 and *fla*17-1 were defective to different extents in the same three polypeptides. Autoradiograms of ^{35}S-labeled polypeptides of 17S sedimenting fractions from flagella of wild-type and mutant strains following one-dimensional electrophoresis at high resolution. First lane in *a* and *b*, proteins from a wild-type strain. Second lane in *a*, proteins from *fla*15. Second and third lane in *b*, proteins from *fla*16 and *fla*17-1. Equal amounts of cpm were analyzed in each lane. Numbers and lines at the left of the figure refer to 13 subunits of 17S complexes. Lines between the two panels indicate the electrophoretic bands that are deficient in each mutant and represent putative subunits of complex A. A dot between the second and third lane in *b* refers to a polypeptide that is present only in 17S sedimenting fractions from *fla*16 and *fla*17-1. Molecular weights of standards are indicated on the right side.

polypeptides from *fla*15 and a wild-type strain revealed that the mutant lacked the majority of two polypeptides of apparent molecular weight 148,000, as well as polypeptides of molecular weights 127,000 and 43,000, respectively (Table III). These four polypeptides are indicated by oblique lines in the maps of polypeptides from wild-type and *fla*15 (Fig. 7, *a* and *b*). Two-dimensional maps of polypeptides from *fla*17-1 had reduced amounts of the same four polypeptides defective in *fla*15 (Fig. 7, *c* and *b*). The new 135,000 apparent molecular weight polypeptide present in *fla*17-1 is indicated by an arrowhead in Fig. 7 *c*. The two-dimensional map of polypeptides from *fla*16 was indistinguishable from that of *fla*17-1.

Three of the polypeptides deficient in *fla*15, *fla*16, and *fla*17-1 were identified as subunits of IFT complex A on the basis of their isoelectric points and apparent molecular weight (Table III). The fourth polypeptide of 43,000 molecular weight that is defective in each mutant could be a previously undetected subunit of IFT complex A.

To determine whether these four polypeptides remain associated in a complex after chromatography and exposure to a high concentration of salt, we performed one- and two-dimensional electrophoresis of wild-type proteins that were eluted by a gradient of NaCl at pH 6.8 from a DEAE-Sepharose column. At least three protein fractions eluted at 0.29–0.30 M NaCl had identical compositions, as assessed by one-dimensional electrophoresis. Polypeptides eluted in that range of NaCl molarity formed a map (Fig. 8) that was simpler than that shown in Fig. 7 *a* but still included the four polypeptides that were deficient from flagella of *fla*15, *fla*16, and *fla*17-1 (Fig. 8), indicated by oblique lines. Therefore, these polypeptides behaved as subunits of a complex that was stable after two subsequent procedures of protein purification.

In addition to these four putative subunits of complex A, 30 other polypeptides were eluted from the column at 0.3 M NaCl and were detectable in the map (Fig. 8). After column chromatography, they remained in proportions similar to those recorded after sedimentation in sucrose gradient (Fig. 7 *a*). Only a subset of these polypeptides were tentatively identified by their apparent molecular weights and isoelectric points as subunits of the IFT complex B, previously described (Cole et al., 1998). Therefore, the molecular composition of complex B may include a larger number of subunits than that reported previously (Cole et al., 1998).

Discussion

To identify the function of components of the machinery that carries out the IFT of particles in *Chlamydomonas*, we have isolated and characterized four ts mutants of flagellar assembly that represent three loci and are defective in the same four characteristics: the flagellar shape, the retrograde velocity of IFT, the frequency of bidirectional IFT, and the concentration of IFT complex A in flagella. This evidence suggests the hypothesis that the complex A is the component of the IFT particles involved in the retrograde transport of proteins within flagella. We also identified a new subunit of the IFT complex A and indicated that the molecular composition of both complex A and complex B includes a number of subunits larger than that reported previously. Finally, to perform this study, we devised a new method for the quantitative analysis of the IFT that measures the velocity as well as the frequency of bidirectional transport and the optical properties of IFT particles. This method will be valuable to determine whether other ts mutants of flagellar assembly are defective in IFT and to identify the structural differences existing between particles moving in opposite directions.

The four mutants of retrograde IFT, *fla*15, *fla*16, *fla*17-1, and *fla*17-2, were selected among 16 strains defective in flagellar assembly for the presence of a characteristic bulge on their flagella. These mutants, like *fla*10, normally have long flagella at the permissive temperature and disassemble or do not regenerate flagella at the restrictive temperature. They are ts in the concentration of complex A in flagella and probably for this reason they are ts in the assembly of flagella. In addition, they are nonconditional for both the occurrence of a bulge of the flagellar membrane and a decrease in the velocity of the retrograde IFT. Four other ts mutants of flagellar assembly, which were isolated in parallel to *fla*15, *fla*16, *fla*17-1, and *fla*17-2, did not

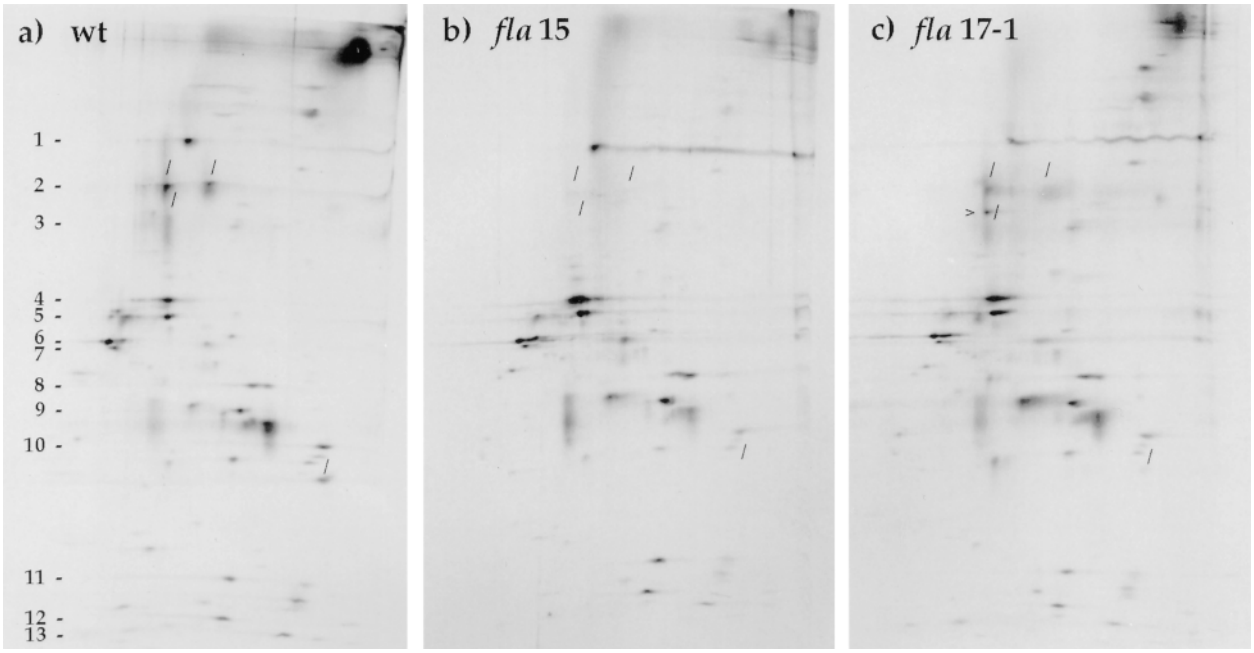

Figure 7. 17S sedimenting fractions from *fla*15 and *fla*17-1 were deficient for the same four polypeptides to a different extent. Autoradiographs of two-dimensional maps of ^{35}S-labeled polypeptides contained in 17S sedimenting fractions from flagella of (*a*) wild-type, (*b*) *fla*15, and (*c*) *fla*17-1. Numbers and lines at the left side of *a* refer to the position of subunits of the 17S complexes, as determined by one-dimensional electrophoresis. Oblique lines in each panel indicate the four polypeptides that are deficient in *fla*15 and *fla*17-1. The new polypeptide present in the 17S sedimenting fractions from *fla*17-1 is indicated by an arrowhead in *c*. Polypeptides appear in the maps in increasing order of acidity from left to right.

present morphological defects of the flagellar membrane nor were they defective in the intraflagellar concentration of complex A. Therefore, the correlation between the phenotype of the bulge and the deficiency in complex A defines a specific subset of ts mutants of flagellar assembly.

The bulge of the flagellar membrane in *fla*15, *fla*16, *fla*17-1, and *fla*17-2 has both a distinct morphology and rare occurrence. In contrast, deformations of the flagellar shape were various and extensive in *fla*14, a short flagella mutant of LC8^{FLA14} (Pazour et al., 1998), and in sea urchin embryos, where ciliary assembly was inhibited (Morris and Scholey, 1997). Furthermore, the bulge of *fla*15, *fla*16, *fla*17-1, and *fla*17-2 occurred once per flagellum and not in every cell and flagellum. This evidence suggested that this phenotype required both a mutation in *FLA*15 or *FLA*16, or *FLA*17 and an unknown defect that occurs once per flagellum and only in a fraction of them.

The deformation of *fla*15, *fla*16, *fla*17-1, and *fla*17-2 flagella also is distinct from that found in *fla*14 for its content. The first was filled with amorphous material that is indistinguishable from the cytoplasm. In contrast, the second contained stacked structures connected to both outer doublet microtubules and the membrane. This material was tentatively identified as the ensemble of complexes A and B (Pazour et al., 1998).

In addition to this morphological defect, we observed a decrease in the velocity of the retrograde IFT in *fla*15, *fla*16, and *fla*17-1 by a new method of quantitative analysis of the IFT that we have developed. Previous analyses of quantitative aspects of IFT were performed by measuring the relative position of individual particles in a series of still-frame video images. This approach was hampered by both the difficulty of identifying the same particle in each frame and the difficulty of detecting particles undergoing retrograde transport. The approach was also laborious because it involved manual processing of individual images. In contrast, the procedure that we have described here involved automatic collection of data from video image sequences lasting over 10-s intervals. The processed linescan data allowed the unambiguous identification of single particles undergoing both anterograde and retrograde transport and the determination of the frequency of bidirectional transport. The numerical data also confirmed the visual perception that the particles undergoing anterograde transport are different in structure and/or size from the particles undergoing retrograde transport. Finally, the use of this procedure allowed us to detect significant changes in the velocity of retrograde IFT in *fla*15, *fla*16, and *fla*17-1.

The occurrence of both the bulge of the flagellar membrane and the substantially slower velocity of retrograde IFT in each mutant was correlated also with a defect in the concentration of the IFT complex A within flagella. Our identification of the flagellar polypeptides deficient in each mutant as subunits of complex A was based on the values of apparent molecular weight and isoelectric point of these polypeptides and on the sedimentation coefficient of the complex that they form. Although the values of these parameters were not identical to those published by others, they were sufficiently close to allow the identification of IFT complex A. We recently confirmed that the electrophoretic band including the two 148,000 molecular

Figure 8. The four polypeptides that are deficient from flagella of *fla*15, *fla*16, and *fla*17-1 behaved as subunits of a complex. Autoradiography of a two-dimensional map of ^{35}S-labeled polypeptides from flagella of a wild-type strain after subsequent sedimentation in sucrose gradient and chromatography in a DEAE-Sepharose column. Oblique lines indicate the four polypeptides that are deficient in *fla*15, *fla*16, and *fla*17-1. Polypeptides appear in the map in increasing order of acidity from left to right.

weight subunits of the 17S complex corresponds to the band including the three p144–p139 subunits of complex A because both bind the monoclonal antibody 139.1 (Cole et al., 1998).

Two other differences between the previous and present characterization of complex A are as follows: first, the IFT complex A characterized here included two rather than three subunits of molecular weight in the 144,000–139,000 range, as reported previously (Cole et al., 1998). Second, a polypeptide of 43,000 apparent molecular weight was deficient in each mutant but was not identified previously as a subunit of either complex A (Cole et al., 1998) or the 17S complex (Piperno and Mead, 1997). These discrepancies could result from differences in the methods of purification and detection of the protein complexes used in these studies. Thus, the third subunit of complex A in the 144,000–139,000 molecular weight range was identified in flagellar extracts that were obtained by exposure to detergent (Cole et al., 1998) rather than by ultrasonic treatment as reported here. Furthermore, the polypeptide of 43,000 molecular weight was identified by autoradiography of ^{35}S-labeled polypeptides that were resolved in two dimensions. It is interesting to note that a polypeptide of molecular weight close to 43,000 was detected by Coomassie blue staining in the immunoprecipitate that included the other subunits of complex A (Fig. 8 *B* by Cole et al., 1998).

Independently from a complete definition of the composition of IFT complex A, three specific characteristics of *fla*15, *fla*16, and *fla*17-1 (namely the distinct bulge of the flagellar membrane, the defect in the concentration of IFT complex A within flagella, and the decrease of retrograde velocity of IFT) occur together as the result of a mutation in any one of three independent loci. This evidence suggests the hypothesis that IFT complex A is involved in retrograde IFT of particles. A defect of the product of *FLA*15, *FLA*16, or *FLA*17 may affect assembly and concentration of complex A and, therefore, the frequency of binding of the complex to a retrograde motor. Alternatively, a structural deficiency of complex A alters the activity of the retrograde motor. In both instances, the velocity of retrograde transport would be decreased.

Phenotypic analysis suggested that *fla*15, *fla*16, and *fla*17-1 affect different aspects of retrograde IFT. The highest defect in the concentration of complex A in flagella of *fla*15 was correlated with the highest deficiency in flagellar regeneration. In contrast, the highest defect in the velocity of retrograde transport in flagella of *fla*17-1 was correlated with the lowest deficiency in flagellar regeneration. The causes of these differences likely will be understood when the molecular identity of the defective gene product of *FLA*15, *FLA*16, and *FLA*17 is determined.

The defective gene product of *FLA*15 could be the subunit of complex A that has the apparent molecular weight 43,000. This subunit of complex A is absent from flagella of *fla*15, whereas the other subunits remain present in trace amounts. If *fla*15 is a null mutant of the 43,000 molecular weight subunit, the assembly of the remaining subunits of complex A may be minimal at the permissive temperature and nonexistent at the restrictive temperature, as we have observed. A similar scenario was described for the radial spoke mutant *pf*24. In this mutant, subunit 2 of the radial spoke stalk was absent, whereas the subunits of the radial spoke head were present in reduced amounts. Furthermore, subunit 2 of the radial spoke stalk was identified as the putative gene product of *PF*24 by both dikaryon rescue and revertant analysis (Huang et al., 1981).

Complexes A and B together likely constitute the particles moving between outer doublet microtubules and flagellar membrane. Three lines of evidence supporting this hypothesis are derived from the characterization of different *fla* mutants. A decrease in the concentration of complex A in flagella of *fla*15, *fla*16, and *fla*17-1 resulted in a decrease in the frequency of bidirectional transport of particles. Furthermore, the deficiency of complexes A and B from flagella of *fla*10 at the restrictive temperature was correlated with a dramatic decrease in the number of particles. Finally, the accumulation of subunits of complexes A and B in flagella of *fla*14 was shown to occur concurrently with the accumulation of particles (Pazour et al., 1998).

Complexes A and B together likely constitute the 17S complex previously described. This identification is supported by the analysis of *fla*10, where KHP1^{FLA10} activity independently was shown to be required for the presence of the 17S complex (Piperno and Mead, 1997) or complex A and complex B within flagella (Cole et al., 1998). The identification also is supported by the evidence described here. 17S sedimenting fractions from the cytoplasmic matrix of *fla*15, *fla*16, and *fla*17-1 flagella included two protein complexes, one of which was identified as complex A.

The number of subunits of complex B may be higher than that reported earlier (Cole et al., 1998). We have

found that chromatography of ^{35}S-labeled 17S sedimenting fractions on a DEAE-Sepharose column followed by two-dimensional electrophoresis of the polypeptides leads to the isolation of 34 molecules, including the subunits of both complexes A and B. Therefore, all of these polypeptides may form complexes that are stable at 0.3 M NaCl, pH 6.8, the salt concentration needed for elution from the column. Some of these molecules were at the limit of autoradiographic detection and, therefore, may represent modified subunits of complexes A and B or polypeptides that remained associated to these complexes in substoichiometric amounts, such as the inner arm subunit p28 (Piperno and Mead, 1997). However, other molecules present in the maps at higher concentration may represent additional subunits of complex B. This hypothesis is also supported by evidence reported by others. The two-dimensional map of the ensemble of complexes A and B prepared by Cole et al. (1998) also included several polypeptides that were as prevalent as identified subunits of complex A or B.

Complex A and a cytoplasmic dynein alone may constitute the whole machinery for retrograde intraflagellar transport. This hypothesis can be confirmed by the analysis of additional mutants. The tight correlation between the occurrence of a specific flagellar bulge and the deficiency of retrograde transport suggests that mutations of retrograde transport in other loci may be identified by the procedure described here. Characterization of the primary defects of these mutants combined with quantitative analyses of intraflagellar transport, such as that reported here, should yield a complete description of the molecular machinery carrying out retrograde transport within flagella.

We are grateful to Michel LeDizet (University of California, Davis, CA) for a critical reading of this manuscript. We also are grateful to Elizabeth Smith (Department of Genetics and Cell Biology, University of Minnesota, St. Paul, MN) for making available the antibody specific for the *PF*16 product and to Joel Rosenbaum, Doug Cole, and Dennis Diener (Department of Molecular Cellular and Developmental Biology, Yale University, New Haven, CT) for making available four monoclonal antibodies to subunits of complexes A and B.

This work was supported by the grant GM-44467 from the National Institutes of Health.

Received for publication July 14 1998 and in revised form 15 October 1998.

References

Adams, G.M., B. Huang, G. Piperno, and D.J. Luck. 1981. Central-pair microtubular complex of *Chlamydomonas* flagella: polypeptide composition as revealed by analysis of mutants. *J. Cell Biol.* 91:69–76.

Adams, G.M.W., B. Huang, and D.L. Luck. 1982. Temperature-sensitive assembly defective flagella mutants of *Chlamydomonas reinhardtii*. *Genetics.* 100:579–586.

Cole, D.G., D.R. Diener, A.L. Himelblau, P.L. Beech, J.C. Fuster, and J.L. Rosenbaum. 1998. *Chlamydomonas* kinesin II–dependent intraflagellar transport (IFT): IFT particles contain proteins required for ciliary assembly in *Caenorhabditis elegans* sensory neurons. *J. Cell Biol.* 141:993–1008.

Golub, G.H., and C. Reinsch. 1970. Singular value decomposition and least squares solutions. *Numer. Math.* 14:403–420.

Harris, E.H. 1989. The *Chlamydomonas* Sourcebook. Academic Press, New York. pp. 780 pp.

Huang, B., G. Piperno, and D.J. Luck. 1979. Paralyzed flagella mutants of *Chlamydomonas reinhardtii*. Defective for axonemal doublet microtubule arms. *J. Biol. Chem.* 254:3091–3099.

Huang, B., G. Piperno, Z. Ramanis, and D.J. Luck. 1981. Radial spokes of *Chlamydomonas* flagella: genetic analysis of assembly and function. *J. Cell Biol.* 88:80–88.

Huang, B., M.R. Rifkin, and D.J. Luck. 1977. Temperature-sensitive mutations affecting flagellar assembly and function in *Chlamydomonas reinhardtii*. *J. Cell Biol.* 72:67–85.

King, S.M., E. Barbarese, J.F. Dillman III, J.H. Patel-King, J.H. Carson, and K.K. Pfister. 1996. Brain cytoplasmic and flagellar outer arm dyneins share a highly conserved M_r 8,000 light chain. *J. Biol. Chem.* 271:19358–19366.

Kozminski, K.G., K.A. Johnson, P. Forscher, and J.L. Rosenbaum. 1993. A motility in the eukaryotic flagellum unrelated to flagellar beating. *Proc. Natl. Acad. Sci. USA*. 90:5519–5523.

Kozminski, K.G., P.L. Beech, and J.L. Rosenbaum. 1995. The *Chlamydomonas* kinesin-like protein *Fla*10 is involved in motility associated with the flagellar membrane. *J. Cell Biol.* 131:1517–1527.

LeDizet, M., and G. Piperno. 1995*a*. *ida4*-1, *ida4*-2 and *ida4*-3 are intron splicing mutations affecting the locus encoding p28, a light chain of *Chlamydomonas* axonemal inner dynein arms. *Mol. Biol. Cell.* 6:713–723.

LeDizet, M., and G. Piperno. 1995*b*. The light chain p28 associates with a subset of inner dynein arm heavy chains in *Chlamydomonas* axonemes. *Mol. Biol. Cell.* 6:697–711.

Luck, D., G. Piperno, Z. Ramanis, and B. Huang. 1977. Flagellar mutants of *Chlamydomonas*: studies of radial spoke-defective strains by dikaryon and revertant analysis. *Proc. Natl. Acad. Sci. USA*. 74:3456–3460.

Malinowski, E.R. 1991. Factor Analysis in Chemistry. John Wiley & Sons, Inc., New York. 350 pp.

McDonald, K. 1984. Osmium ferricyanide fixation improves microfilament preservation and membrane visualization in a variety of animal cell types. *J. Ultrastruct. Res.* 86:107–118.

Morris, R.L., and J.M. Scholey. 1997. Heterotrimeric kinesin-II is required for the assembly of motile 9+2 ciliary axonemes on sea urchin embryos. *J. Cell Biol.* 138:1009–1022.

Pazour, G.J., C.G. Wilkerson, and G.B. Witman. 1998. A dynein light chain is essential for retrograde particle movement of intraflagellar transport (IFT). *J. Cell Biol.* 141:979–992.

Piperno, G. 1995. Cilia and flagella. *Methods Cell Biol*. 47:107–112.

Piperno, G., and K. Mead. 1997. Transport of a novel complex in the cytoplasmic matrix of *Chlamydomonas* flagella. *Proc. Natl. Acad. Sci. USA*. 94:4457–4462.

Piperno, G., Z. Ramanis, E.F. Smith, and W.S. Sale. 1990. Three distinct inner dynein arms in *Chlamydomonas* flagella: molecular composition and location in the axoneme. *J. Cell Biol.* 110:379–389.

Piperno, G., K. Mead, and S. Henderson. 1996. Inner dynein arms but not outer dynein arms require the activity of kinesin homologue protein KHP1^{FLA10} to reach the distal part of flagella in *Chlamydomonas*. *J. Cell Biol.* 133:371–379.

Press, W.H., S.A. Teukolski, W.T. Vetterling, and B.P. Flannery. 1992. Numerical Recipes in C: The Art of Scientific Computing. Cambridge University Press, Cambridge, UK. 994 pp.

Sager, R., and S. Granick. 1953. Nutritional studies with *Chlamydomonas reinhardtii*. *Ann. NY Acad. Sci.* 466:18–30.

Scholey, J.M. 1996. Kinesin-II, a membrane traffic motor in axons, axonemes, and spindles. *J. Cell Biol.* 133:1–4.

Smith, E.F., and P.A. Lefebvre. 1996. PF16 encodes a protein with armadillo repeats and localizes to a single microtubule of the central apparatus in *Chlamydomonas* flagella. *J. Cell Biol.* 132:359–370.

Walther, Z., M. Vashishtha, and J.L. Hall. 1994. The *Chlamydomonas FLA10* gene encodes a novel kinesin-homologous protein. *J. Cell Biol.* 126:175–188.